JAST, Vol. 13, No. 2, pp.

JAST
Journal of Aerospace Science and Technology

Scientific-Research Article

Numerical and experimental analysis of Ballistic behavior of ceramic-reinforced Aluminum matrix composites plates

Ali Ansari[1], Jafar Eskandari Jam[2], Ali Alizadeh[3], Mohsen Heydari Beni[4], Majid Eskandari Shahraki[5]
1,2 and 4- Faculty of Mechanical Engineering, Malek Ashtar University of Technology, Tehran
3- University Complex of Materials and Manufacturing Technologies, Malek Ashtar University of Technology, Tehran,
5- Faculty of Aerospace Engineering, Ferdowsi University of Mashhad
* Tehran, zip code: 15875-1774.

Email: * eskandari@mut.ac.ir

This study was designed to investigate the ballistic behavior of ceramic-reinforced aluminum composite plates numerically and experimentally and to present an optimal sample design. The parameters studied were ceramic reinforcement percentage and type of matrix alloy. This study used the matrix alloys 6061, 7075, and 5083. The percentage of ceramics used in this study is 15, 30, and 45% by weight. The samples are in three thicknesses of 20, 25, and 30 mm. 27 simulated samples were numerically analyzed with Abaqus finite element software in this study based on existing ballistic protection criteria, one then determines the optimal numerical sample. Using the squeeze casting method, a laboratory sample has been made and experimentally tested to evaluate the numerical results. Lastly, the numerical analysis and the experimental test were compared and the optimal sample was determined.

Keywords: *Ballistic, Aluminum Matrix Composite, Ceramic, Finite Elements, Armor*

Introduction

Metal matrix composites have gained attention in recent years due to their strength, stiffness, and low density. Producing metal matrix composites is an attempt to combine the appropriate properties of metals with those of ceramics. As a result of adding high refractory particles with high strength to a ductile metal matrix, the material has mechanical characteristics intermediate between those of a matrix alloy and that of ceramic. When these characteristics are combined, a material with ideal properties is obtained [1].

Silva et al. (2014) studied the mechanical and ballistic properties of alumina ceramics for armor applications. Alumina plates with thicknesses of 10 mm were created with compositions including 92, 96, and 99% Alumina. This study followed NIJ-0108.01 (Special projectile standard with 7.62 * 51 calibers). The results showed that neither of the shots caused deformation nor penetration in the witness plate that was behind the 92% alumina plate, which indicated that the ceramic has a high ballistic

1 M.Sc.
2 Professor
3 Associate Professor
4 Ph.D. student
5 Ph.D. student

Received Date: 9 Oct. 2020
Accepted Date: 15 Feb. 2021 Print ISSN: 1735-2134

application potential, being able to withstand impacts with more than 4000 joules. [2]

Rashed et al. (2011) studied multi-layered ceramic and metal armors with a polymeric interlayer for high-speed impacts. Two-dimensional and three-dimensional models of multi-layered armor were simulated and analyzed in this study. The study concluded that dual-layer armor has the best ballistic performance among other layered armors. In addition, it was found that measuring penetration depth and residual velocity of the projectile is an efficient method of evaluating an armor's ballistic performance. [3]

Iqbal et al. (2016) investigated Armox 500T steel's behavior under different temperatures and strain rates when facing armor-piercing incendiary projectiles. The study used both numerical and experimental methods. Projectiles' calibers were 7.62 and 12.7, their speed was 830 m/s, and the thickness of the samples was 8 and 10 mm. As a result, it has been found that as stress triaxiality increases, the fracture strain of this steel decreases, and yield strength increases with increasing strain rate. Additionally, it was found that the projectile material is not sensitive to stress triaxiality and strain rate. [4]

Venkatesan et al. (2017) performed a numerical study and comparison of the ballistic performance of bilayer alumina/aluminum and silicon carbide/aluminum armor against blunt nose projectiles. The structural model and Johnson-Holmquist damage model were used in this study to calculate the strength and fracture state of brittle materials like silicon carbide and alumina, and the structural model and Johnson-Holmquist damage model was used to calculate the strength and fracture state of steel and aluminum. the results showed that Silicon/carbide armor outperformed aluminum/alumina armor in ballistic tests. [5]

Based on researches conducted since 1988, Cui et al. (2017) examined the effect of ceramic properties, penetration depth, and test parameters such as ceramic tile thickness and projectile speed on the ballistic performance of ceramic armor. In this study, ceramics such as Al2o3, SIC, B4C, and TiB2 were used. Ceramic armor's ballistic performance was significantly influenced by the type of ceramic, the thickness of the tile, and the speed of the projectile. In addition, ceramic armor's mechanical properties have a strong correlation with its ballistic performance. [6]

Liu et al. (2018) carried out a numerical study of the efficacy of ceramic balls in protecting Ultra-High-Performance concrete from high-speed rigid projectiles utilizing Smoothed Particle Hydrodynamics method. Based on validated numerical models, parametric studies were conducted in this study to examine the effects of diameter, spatial arrangement, and material type of ceramic balls. As compared to concrete samples that were hit by projectiles with a speed of 500 to 850 m/s, the samples that were protected by six layers of ceramic balls with a diameter of 6 mm and a hexagonal structure had the lowest penetration depth. [7]

The ballistic performance of ceramic/metal tiles in the inter tile gaps and the projectile impact position were studied experimentally by Seifert et al. (2019). This research used carbide core projectiles. The results showed that the residual velocity of the projectile after hitting the tile/tungsten edge was 7.62 times higher than when the projectile hit the inter-tile gap. As the adhesive stiffness decreases and the gap width widens, the ballistic strength also drops dramatically. [8]

Tian et al. (2019) conducted a numerical and experimental investigation into the effect of metallic frame materials on the strength of ceramic-metal hybrid structures. zirconia-toughened alumina ceramic composite ingots in this study are made of 7075 aluminum, 4340 steel, and TC4 titanium. Results showed that hybrid structures made from titanium alloy TC4 and 4340 steel had respectively the highest and lowest penetration resistance. [9]

Tian et al. (2019) conducted a numerical and experimental investigation on the effect of ceramic constraints on the protective performance of ceramic-metal hybrid structures under impact loads. These three parameters have been studied in this research: the size of the ceramics, the boundary conditions, and the connection mode of the substructures. The parameters of boundary conditions and the connection mode of the substructures were also found to be relatively important constraints in improving the performance of ceramic ingots. However, boundary conditions have little effect on these structures' penetration resistance. [10]

Fras et al. (2019) performed experimental and numerical studies of dynamic perforation of steel armor with very high strength. The projectiles in this study were 240 to 380 meters per second fast, weighed 14 grams, and had three shapes of noses: blunt, hemispherical, and conical. After hitting the targets, Conical and Blunt projectiles were deformed, giving them a final shape similar to a

hemispherical projectile. The exit speed of projectiles with more blunt noses was found to be 10% faster than that of projectiles with conical noses. Blunt nose projectiles are therefore more effective than conical projectiles. [11]

Based on the result of researches in the field of armor systems, it has been determined that to overcome the kinetic energy of a projectile, the armor surface must be very hard so that the projectile nose would break and flatten when it collides. In addition to ceramic materials, the next layers must possess high fracture toughness in order to absorb and dissipate the projectile's kinetic energy. For the armor to be as light as possible, the materials need to be light.

One of the research gaps in most of the studies was that the armors could only withstand one shot because of the ceramic layer's monolithic nature. Furthermore, researchers agree that integrated armors have better ballistic performance than layered armors, but the majority of composite armors are designed as layered, which is the subject of this study and seeks to solve these two challenges. This is the article's innovation in comparison to previous studies.

Research Methods

Numerical simulation

In this research, the vertical impact of a 7.62 caliber projectile with a speed of 800 m/s was studied on a target made of an aluminum matrix composite with alumina ceramic reinforcing particles as well as the penetration of the projectile. This research is aimed at finding the optimal thickness and weight of the composite target as well as examining the effect of the aluminum alloy material used as the base and the proportion of alumina used in the composite. Table (1) lists the problem variables. Due to the axi-symmetric nature of the target object and projectile, the simulated set is only a quarter of the configuration. Based on researches, the jackets of the brass and copper projectiles barely affect penetration [12&13]. Therefore, only the core of the projectile is simulated. Figure (1) shows the geometry of the projectile simulated in the software.

Table (1) - Problem variables

	Effective factors			
1	Alumina weight percentage (%)	45	30	15
2	Target thickness (mm)	30	25	20
3	Type of aluminum alloy	Al7075	Al5083	Al6061

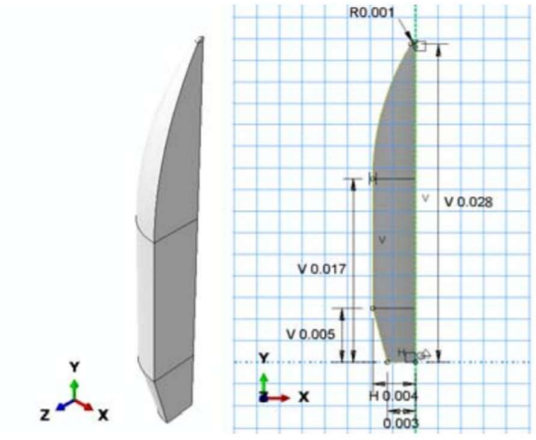

Figure (1) - Projectile geometry

Figure (2) illustrates the geometry of the aluminum matrix in front of the target that has been designed in the software. Every aluminum layer has a thickness of 2 mm, a length and width of 67 mm, a radius of 1 mm for each hemisphere, and a distance of 0.4 mm between each cavity.

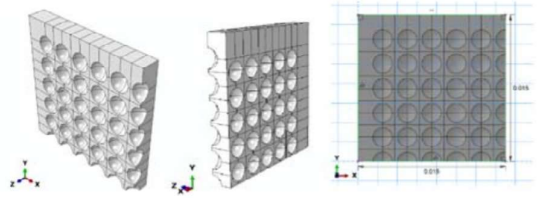

Figure (2) - Geometry of aluminum matrix in front of the target

Figure (3) shows the geometry of the aluminum back of the target. The aluminum back thickness varies in each of the simulated samples depending on the percentage and thickness of the ceramic sample.

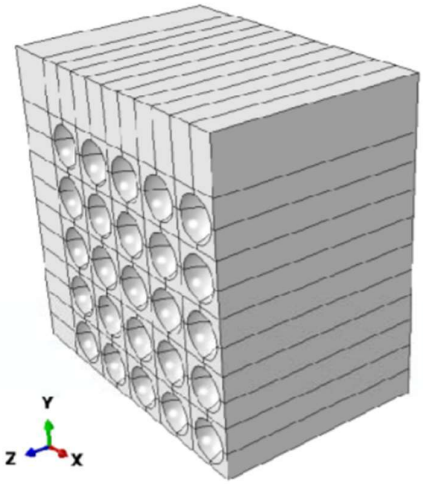

Figure (3) - Geometry of the target backing Aluminum

For ballistic analysis of the simulated sample, it is necessary to determine the Johnson-Cook model parameters for ductile materials (aluminum and steel alloys) and the Drucker-Prager model parameters, and the Mie-Gruneisen equation of state for brittle materials (alumina).

For the interaction between the projectile and the target, a contact constraint must be established. Due to penetration, the contact constraint used in this research is between the interior surfaces of the projectile and the target. Creating this type of contact constraint is not supported in the CAE environment, so commands are entered manually in the model input file.

As a result of the symmetry condition in the target and projectile symmetry levels, the symmetry boundary condition is used. For the target's lateral surfaces, the degrees of freedom are also closed in all directions to be close to the real conditions of the experimental test. The projectile speed is 800 m/s in the negative direction of the axis.

A key problem of the finite element method is finding the optimal number of elements for meshing. because by increasing the number of model elements in this method, the simulation results are converged and are more accurate. however, as the number of elements increases, the convergence speed decreases. This means that when the number of elements exceeds a certain number, the simulation result does not improve significantly, but the problem analysis time also increases dramatically, and most of the time the results are diverged. Therefore, in order to determine the optimal number of elements, the number of elements is increased gradually, and as soon as the results do not change substantially as the number of elements increases, this operation stops, and that number of elements is considered the optimal number. According to the number or size of elements, the residual velocity graph is used to determine the optimal number of elements. The number of optimal elements is first calculated for the target, and then it is calculated for the projectile. As for the size of the optimal element in the target, it is 0.35 mm, and in the projectile, it is 0.40 mm. Changing the size of the projectile elements from 0.40 mm to 0.35 mm does not significantly affect the residual velocity, so the size of the projectile elements is also assumed to be 0.35 mm. Figures (4) and (5) show the residual velocity graphs in terms of the target element and projectile size.

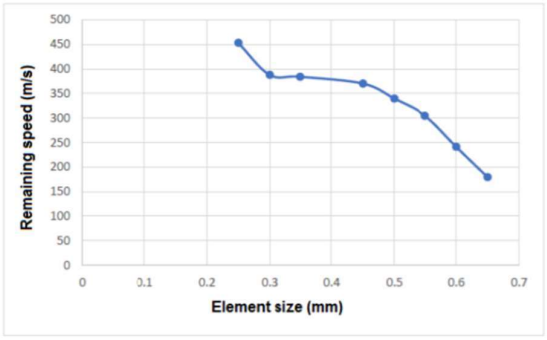

Figure (4) – The graph of the projectile residual velocity in terms of the target elements size

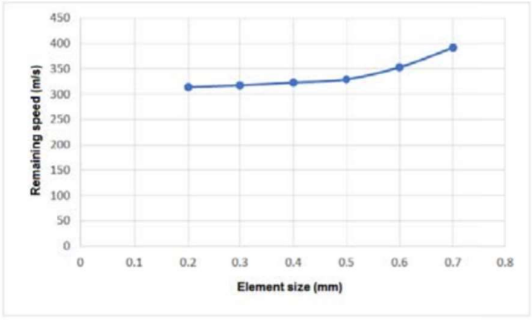

Figure (5) – The graph of the projectile residual velocity in terms of the projectile elements size

Sample making

The 99.5% alumina spheres and 5083 aluminum are used to create aluminum matrix composite samples reinforced with alumina. In order to make the sample by squeeze casting method, the mold surfaces must first be cleaned with acetone in order

to avoid contamination on the surface. Once the mold has been sprayed with lubricant, it is placed inside the furnace, and the mold and furnace are then placed in the press machine. Then, the furnace is turned on until the mold temperature reaches 580 ° C. Once the mold has heated up, the aluminum ingots in the crucible and the crucible are taken into other furnaces and the furnace is turned on to melt the aluminum ingots. Melting aluminum is poured into the mold and onto the ceramic reinforcements after preheating the mandrel. Following that, 60 tons of pressure is applied to it by the press machine. The furnace chamber and press machine are shown in figure (6).

Figure (6) - Press machine and furnace chamber

Once the molten aluminum has solidified, the pressure is removed from the sample. Eventually, the sample mold comes out after cooling. Figure (7) shows the created sample.

Figure (7) - three-point flexural test conducted on the composite plate

Ballistic evaluation of the c sample

Fixing the created sample in a place with a fixture ensures that the support has no degree of freedom. An Ak-471 is then used to fire a projectile with a size of 39 * 7.62 steel core from a distance of 15 meters. The projectile speed is 740 m/s. Three samples were prepared and hit by the projectile to ensure the test results. Figure (8) shows the projectile used.

Figure (8) - projectile with a size of 7.62×39

Numerical method results

The projectile penetration process in samples with a thickness of 30 mm and 45% ceramic

As mentioned previously, three types of aluminum were used as the matrix material to simulate composite samples; aluminum 6061, 7083, and 5083, each of which is listed below. As shown in Figure (9), the projectile completely passed through

1 Avtomat Kalashnikova

the sample with 6061 aluminum matrix, and this sample is unable to stop the projectile. In Figures (10) and (11) the projectile is stopped by simulated samples consisting of two types of aluminum matrices, 7075 and 5083.

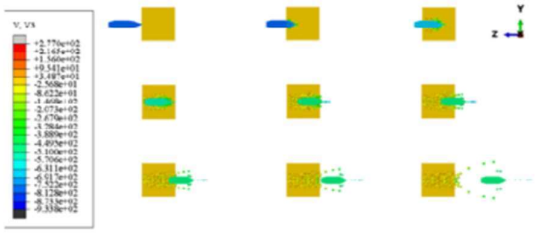

Figure (9) - Speed distribution in the projectile penetration process in the sample with 6061 aluminum matrix

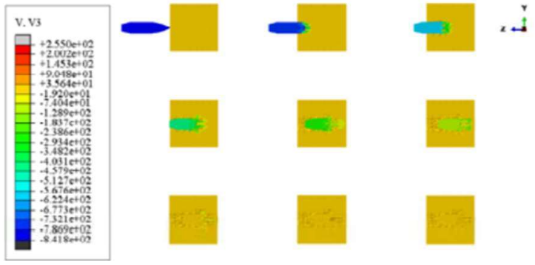

Figure (10) - Speed distribution in the projectile penetration process in the sample with 7075 aluminum matrix

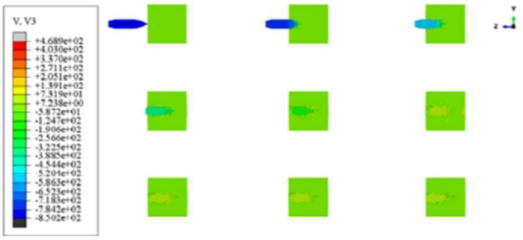

Figure (11) - Speed distribution in the projectile penetration process in the sample with 5083 aluminum matrix

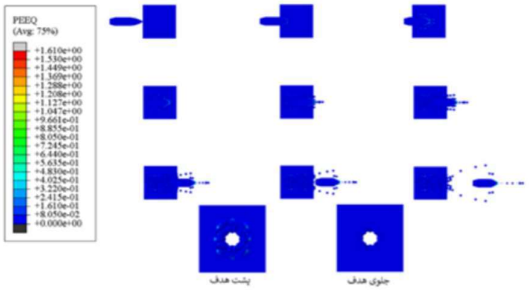

Figure (12) - Distribution of plastic strain equivalent to the sample with 6061 aluminum matrix

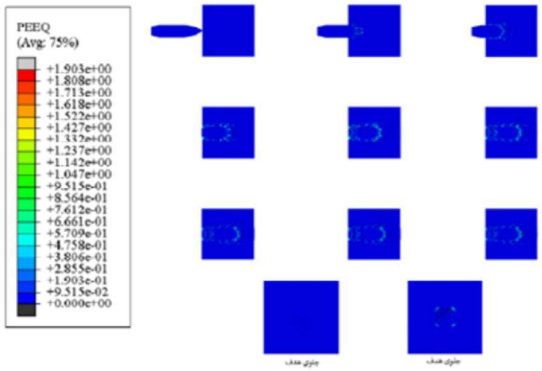

Figure (13) - Distribution of plastic strain equivalent to the sample with 7075 aluminum matrix

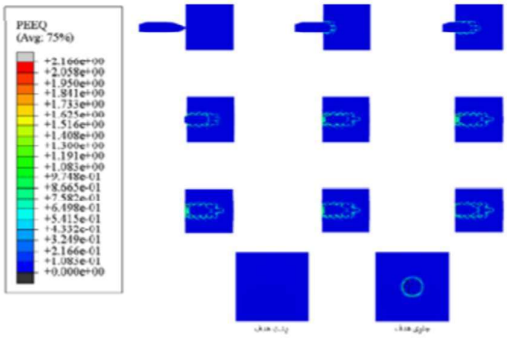

Figure (14) - Distribution of plastic strain equivalent to the sample with 5083 aluminum matrix

The projectile penetration process in samples with a thickness of 30 mm and 30% ceramic

Figures (15), (16), and (17) show the speed distributions for samples with three aluminum matrices (6061, 7075, and 5083, respectively). As can be seen, the projectile passes through the sample with 6061 aluminum matrix. The projectile stopped after penetrating the sample with 7075 aluminum matrix, but the damage caused by the impact and penetration of the projectile reached the surface

behind the sample. The sample with 5083 aluminum matrix stops the projectile.

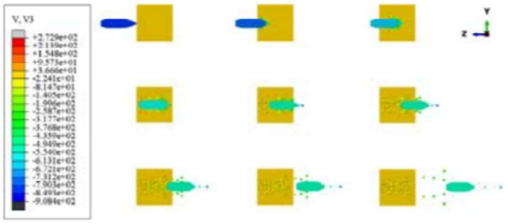

Figure (15) - Speed distribution in the projectile penetration process in the sample with 6061 aluminum matrix

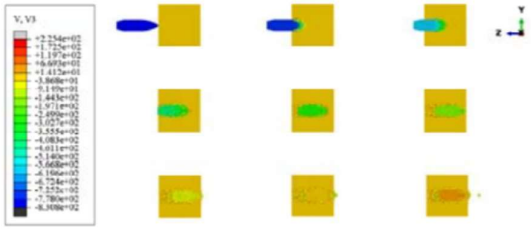

Figure (16) - Speed distribution in the projectile penetration process in the sample with 7075 aluminum matrix

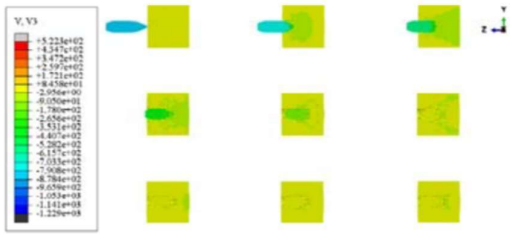

Figure (17) - Speed distribution in the projectile penetration process in the sample with 5083 aluminum matrix

Figures (18) (19) and (20) show the equivalent plastic strain distribution and the front and back surfaces of the samples after projectile impact. It can be seen in Figure (23) that in the sample with 7075 aluminum matrix, the damage caused by the impact and penetration of the projectile reached the surface behind the sample and was completely damaged across its thickness.

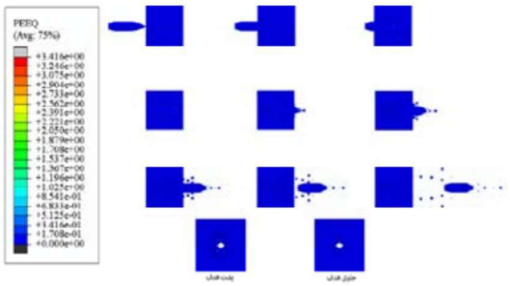

Figure (18) - Distribution of plastic strain equivalent to the sample with 6061 aluminum matrix

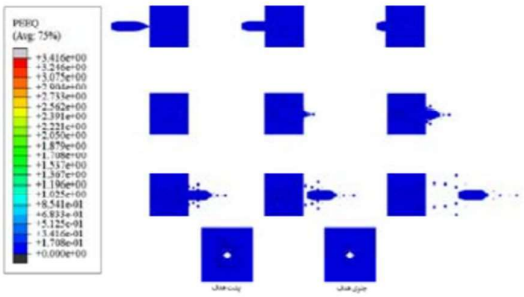

Figure (19) - Distribution of plastic strain equivalent to the sample with 7075 aluminum matrix

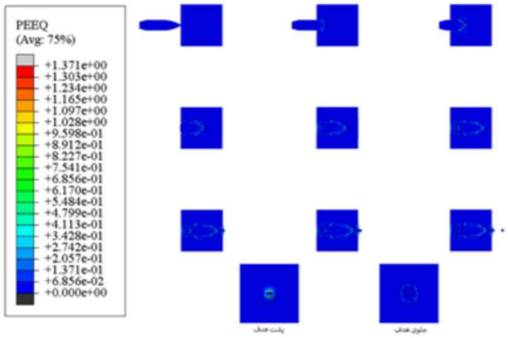

Figure (20) - Distribution of plastic strain equivalent to the sample with 5083 aluminum matrix

The projectile penetration process in samples with a thickness of 11 mm and 35% ceramic

Figures (21) and (22) show the speed distribution in the sample with 6061 and 7075 aluminum matrices, respectively. both samples are perforated by Impact and penetration of the projectile, and the projectile passes through them. Figure (23) also shows the speed distribution in the sample with 5083 matrix.

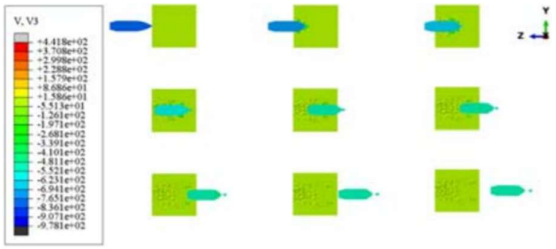

Figure (21) - Speed distribution in the projectile penetration process in the sample with 6061 aluminum matrix

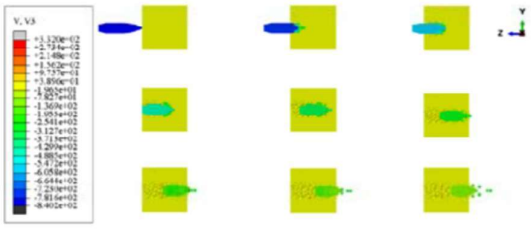

Figure (22) - Speed distribution in the projectile penetration process in the sample with 7075 aluminum matrix

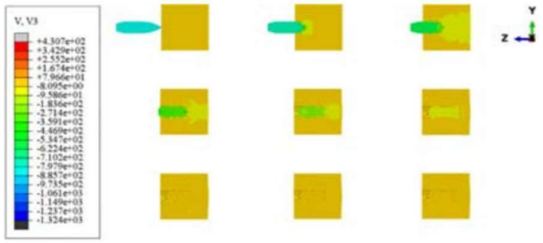

Figure (23) Speed distribution in the projectile penetration process in the sample with 5083 aluminum matrix

Figures (24), (25), and (26) show the equivalent plastic strain and the surfaces of the samples after the projectile had struck them.

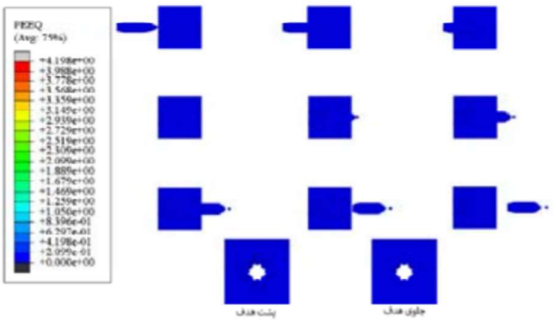

Figure (24) - Distribution of plastic strain equivalent to the sample with 6061 aluminum matrix

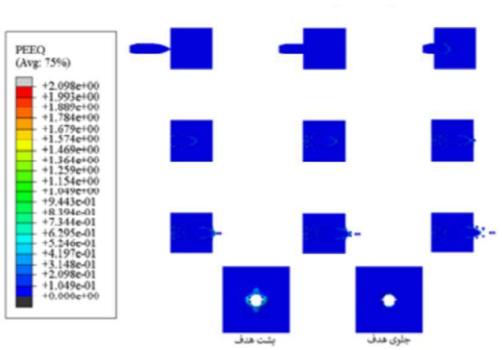

Figure (25) - Distribution of plastic strain equivalent to the sample with 7075 aluminum matrix

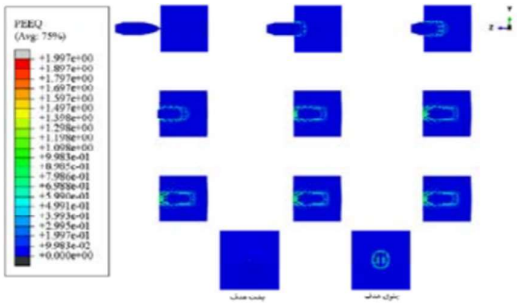

Figure (26) - Distribution of plastic strain equivalent to the sample with 5083 aluminum matrix

The projectile penetration process in samples with a thickness of 25 mm and 45% ceramic

As shown in Figure (27), the projectile completely penetrates and passes through the sample with 6061 aluminum matrix.

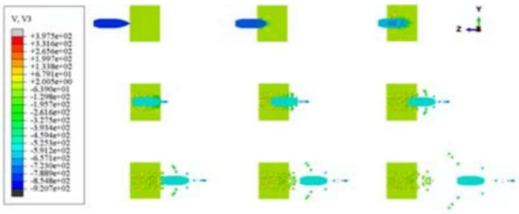

Figure (27) - Speed distribution in the projectile penetration process in the sample with 6061 aluminum matrix

Figure (28) shows the speed distribution in the projectile penetration process in the sample with 7075 aluminum matrix. After the projectile penetrated this sample, it stopped, but the damage caused by its penetration reached the surface behind it.

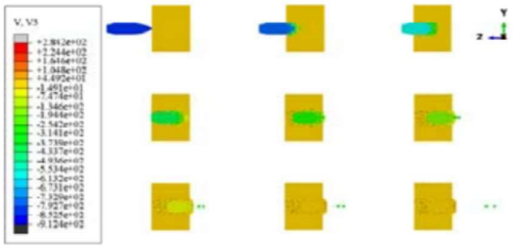

Figure (28) - Speed distribution in the projectile penetration process in the sample with 7075 aluminum matrix

Figure (29) shows the projectile penetration process in the sample with 5083 aluminum matrix. The projectile stopped after hitting this sample, as can be seen in the image.

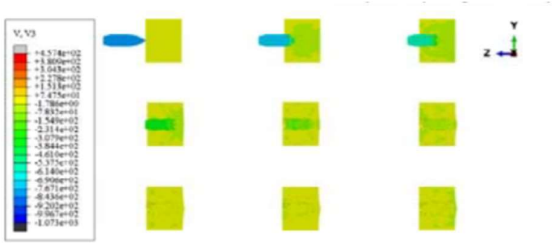

Figure (29) - Speed distribution in the projectile penetration process in the sample with 5083 aluminum matrix

In Figures (30), (31), and (32), the equivalent plastic strain distribution is observed in the samples with 6061, 7075, and 5083 aluminum matrices when the projectile penetrates them.

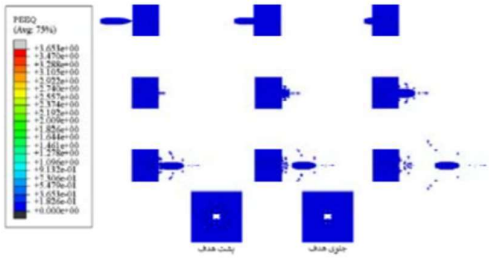

Figure (30) - Distribution of plastic strain equivalent to the sample with 6061 aluminum matrix

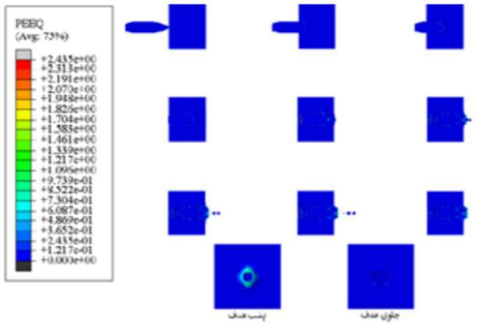

Figure (31) - Distribution of plastic strain equivalent to the sample with 7075 aluminum matrix

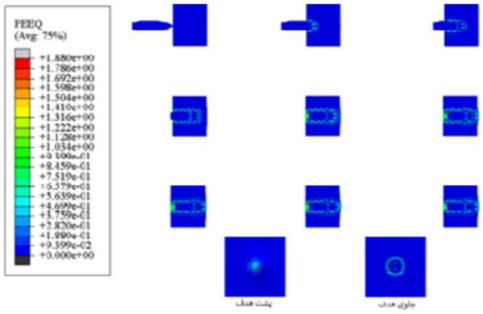

Figure (32) - Distribution of plastic strain equivalent to the sample with 5083 aluminum matrix

The projectile penetration process in samples with a thickness of 25 mm and 30% ceramic

Figures (33), (34), and (35) show the speed distribution in the projectile penetration process in samples with 6061, 7075, and 5083 aluminum matrices, respectively. The projectile was stopped by 5083 aluminum matrix only after it collided and penetrated the sample. In Figures (36), (37), and (38), the equivalent plastic strain distribution is observed in samples with aluminum matrices 6061, 7075, and 5083 when the projectile penetrates them.

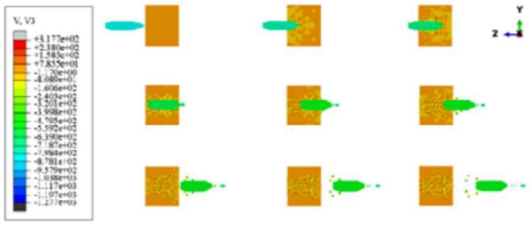

Figure (33) - Speed distribution in the projectile penetration process in the sample with 6061 aluminum matrix

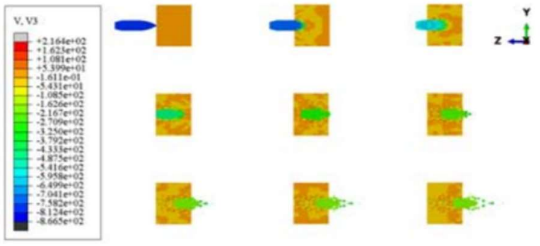

Figure (34) - Speed distribution in the projectile penetration process in the sample with 5075 aluminum matrix

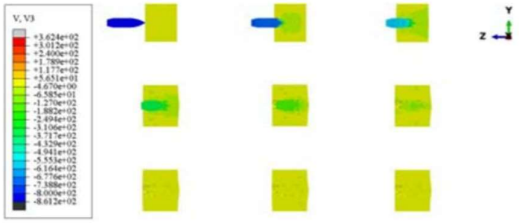

Figure (35) - Speed distribution in the projectile penetration process in the sample with 5083 aluminum matrix

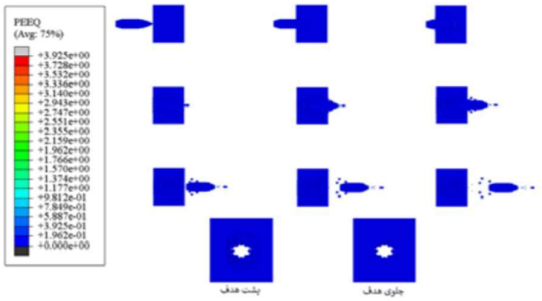

Figure (36) - Distribution of plastic strain equivalent to the sample with 6061 aluminum matrix

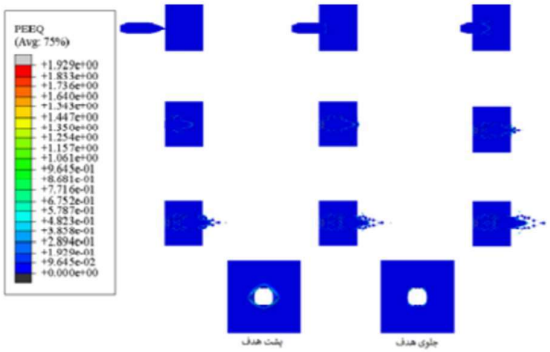

Figure (37) - Distribution of plastic strain equivalent to the sample with 7075 aluminum matrix

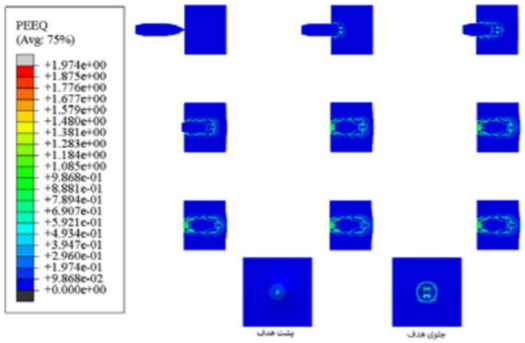

Figure (38) - Distribution of plastic strain equivalent to the sample with 5083 aluminum matrix

The projectile penetration process in samples with a thickness of 25 mm and 15% ceramic

Figures (39), (40), and (41) show the speed distribution in the projectile penetration process in samples with 6061, 7075, and 5083 aluminum matrices, respectively. As can be seen, the projectile did not stop in any of the samples and passed through all three of them.

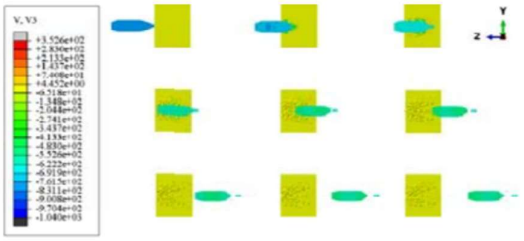

Figure (39) - Speed distribution in the projectile penetration process in the sample with 6061 aluminum matrix

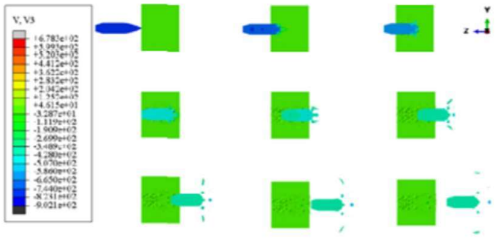

Figure (40) - Speed distribution in the projectile penetration process in the sample with 7075 aluminum matrix

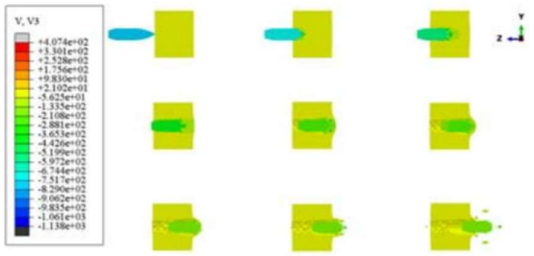

Figure (41) - Speed distribution in the projectile penetration process in the sample with 5083 aluminum matrix

Figures (42), (43), and (44) show the equivalent plastic strain distribution and the front and back surfaces of samples 6061, 7075, and 5083 after the projectile impact, respectively. As can be seen, all the samples were completely damaged across their thickness and the projectile completely passed through the samples.

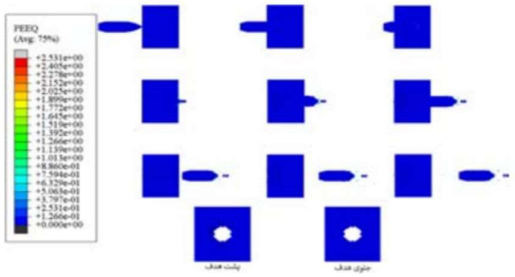

Figure (42) - Distribution of plastic strain equivalent to the sample with 6061 aluminum matrix

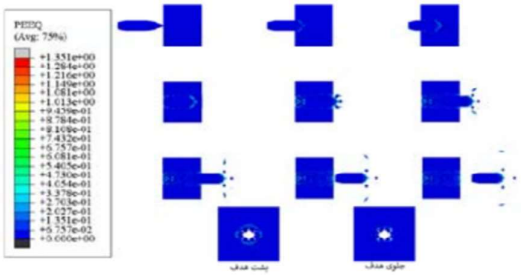

Figure (43) - Distribution of plastic strain equivalent to the sample with 7075 aluminum matrix

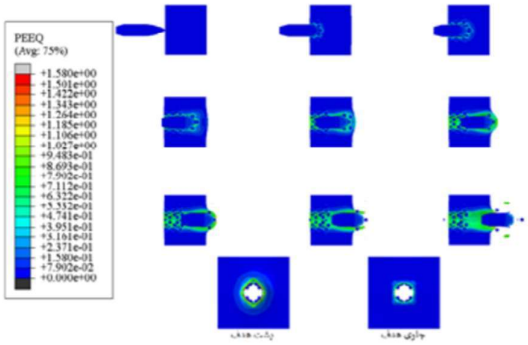

Figure (44) - Distribution of plastic strain equivalent to the sample with 5083 aluminum matrix

The projectile penetration process in samples with a thickness of 21 mm and 65% ceramic

Figures (45), (46), and (47) show the speed distribution in the projectile penetration process in the samples with 6061, 7075, and 5083 aluminum matrices, respectively. Here, as in the previous section, it can be seen that the projectile did not stop in any of the samples and passed through all three.

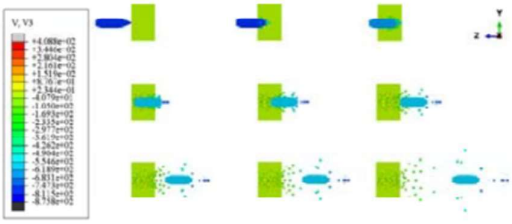

Figure (45) - Speed distribution in the projectile penetration process in the sample with 6061 aluminum matrix

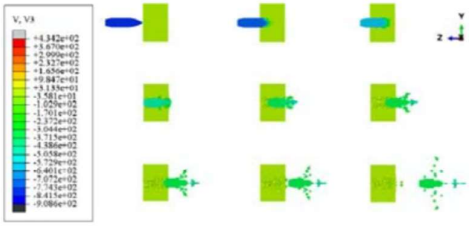

Figure (46) - Speed distribution in the projectile penetration process in the sample with 7075 aluminum matrix

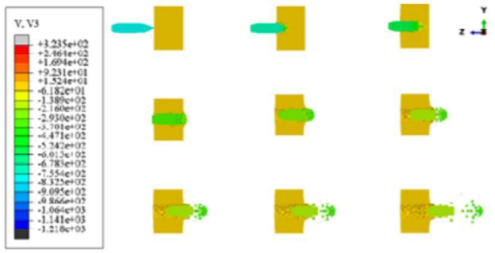

Figure (47) - Speed distribution in the projectile penetration process in the sample with 5083 aluminum matrix

Figures (48), (49), and (50) show the equivalent plastic strain distribution and the front and back surfaces after the impact of the projectile in 6061, 7075, and 5083 aluminum matrix samples, respectively.

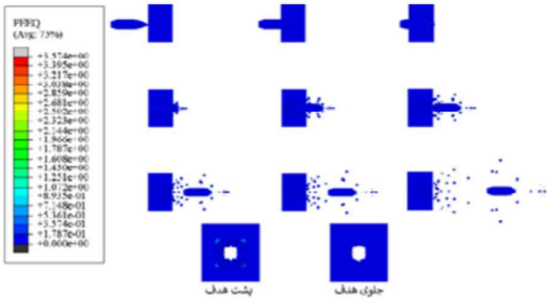

Figure (48) - Distribution of plastic strain equivalent to the sample with 6061 aluminum matrix

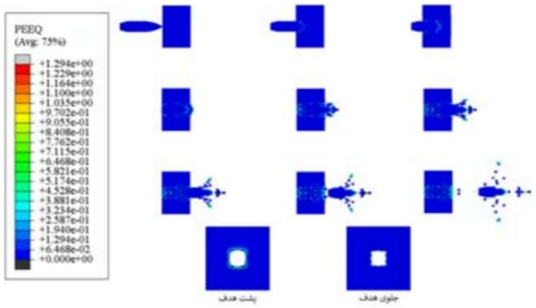

Figure (49) - Distribution of plastic strain equivalent to the sample with 7075 aluminum matrix

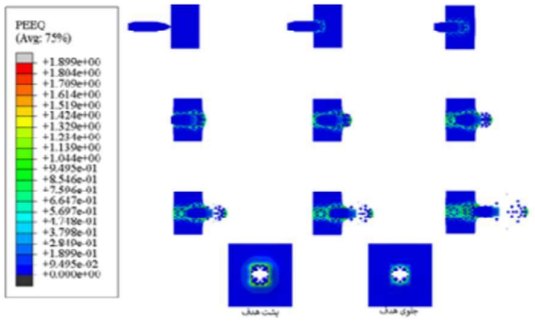

Figure (50) - Distribution of plastic strain equivalent to the sample with 5083 aluminum matrix

The projectile penetration process in samples with a thickness of 20 mm and 30% ceramic

Figures (51), (52), and (53) show the speed distribution in the projectile penetration process in samples with 6061, 7075, and 5083 aluminum matrices, respectively. Here, as in the previous section, it can be seen that the projectile did not stop in any of the samples and passed through all three.

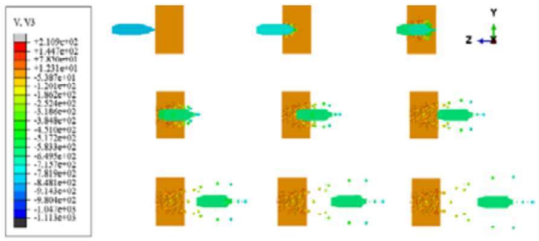

Figure (51) - Speed distribution in the projectile penetration process in the sample with 6061 aluminum matrix

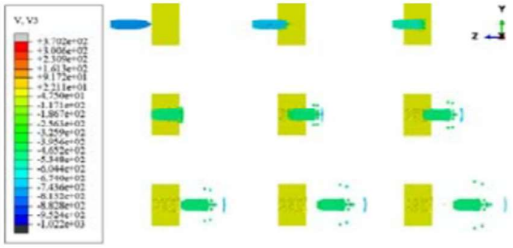

Figure (52) - Speed distribution in the projectile penetration process in the sample with 7075 aluminum matrix

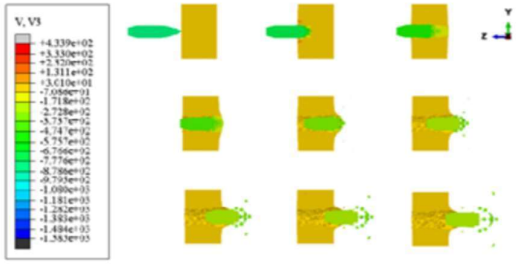

Figure (53) - Speed distribution in the projectile penetration process in the sample with 5083 aluminum matrix

Figures (54), (55) and (56) show the equivalent plastic strain distribution, the front and back surfaces of the samples with 6061, 7075, and 5083 aluminum matrices.

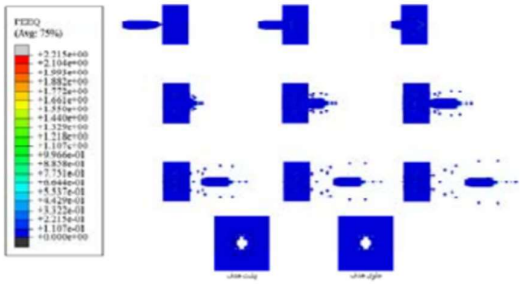

Figure (54) - Distribution of plastic strain equivalent to the sample with 6061 aluminum matrix

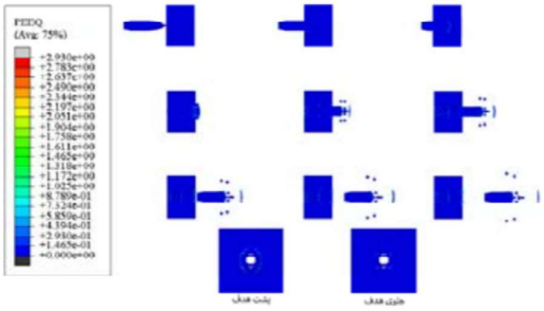

Figure (55) - Distribution of plastic strain equivalent to the sample with 7075 aluminum matrix

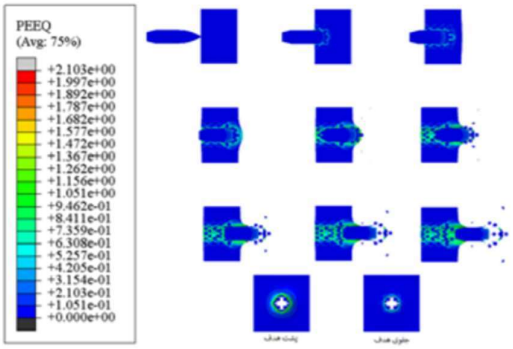

Figure (56) - Distribution of plastic strain equivalent to the sample with 5083 aluminum matrix

The projectile penetration process in samples with a thickness of 20 mm and 15% ceramic

Figures (57), (58), and (59) show the speed distribution in the projectile penetration process, respectively, in samples with 6061, 7075, and 5083 aluminum matrices. As can be seen, the projectile did not stop in any of the samples and passed through all three of them.

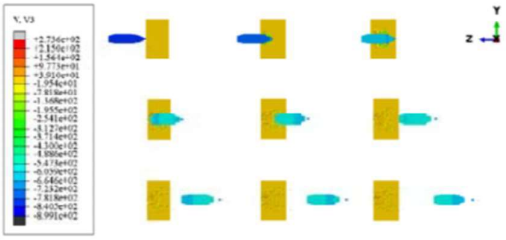

Figure (57) - Speed distribution in the projectile penetration process in the sample with 6061 aluminum matrix

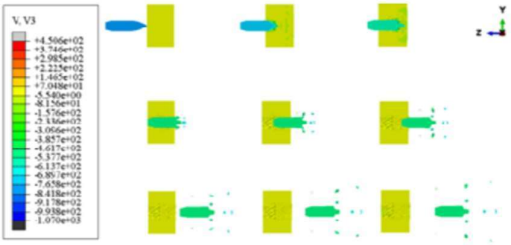

Figure (58) - Speed distribution in the projectile penetration process in the sample with 7075 aluminum matrix

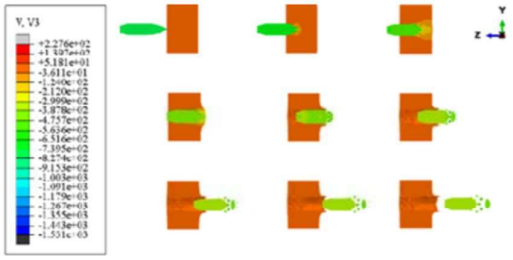

Figure (59) - Speed distribution in the projectile penetration process in the sample with 5083 aluminum matrix

Figures (60), (61) and (62) show the equivalent plastic strain distribution, the front and back surfaces of the samples with 6061, 7075, and 5083 aluminum matrices.

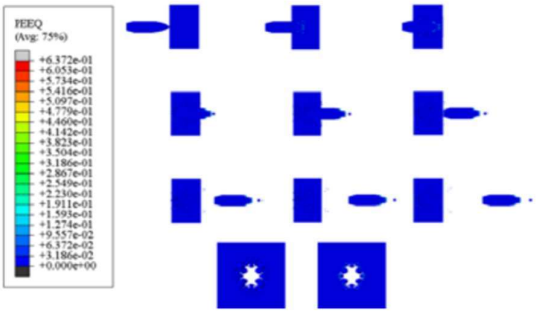

Figure (60) - Distribution of plastic strain equivalent to the sample with 6061 aluminum matrix

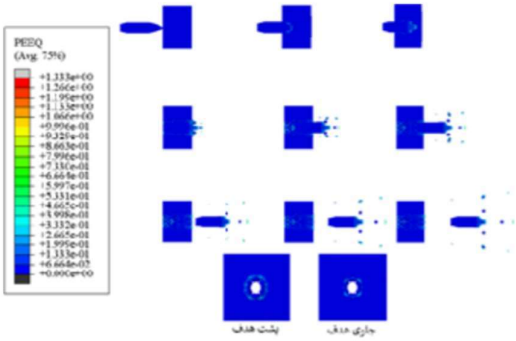

Figure (61) - Distribution of plastic strain equivalent to the sample with 7075 aluminum matrix

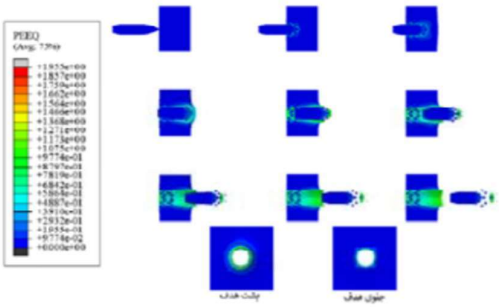

Figure (62) - Distribution of plastic strain equivalent to the sample with 5083 aluminum matrix

The effect of ceramic percentage on the speed and kinetic energy of the projectile in collision with samples with a thickness of 20 mm

The speed and kinetic energy of the projectile does not significantly decrease in the sample with 6061 aluminum matrix with a thickness of 20 mm, and the projectile passes through the sample and damages it severely. Therefore, increasing the ceramics percentage does not have a significant effect on reducing speed and kinetic energy. The rate of reduction in the projectile speed and kinetic energy in collision with this sample in different percentages of ceramics is seen in Figure (63).

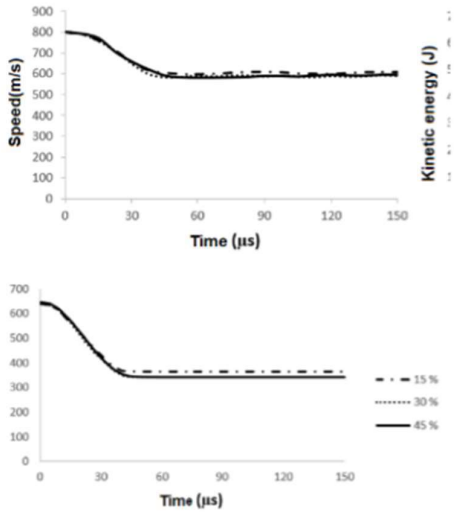

Figure (63) - The graph of the projectile speed and kinetic energy in the sample with 6061 aluminum matrix and a thickness of 20 mm

Increasing the percentage of ceramics in the sample with 7075 aluminum matrix with a thickness of 20 mm caused the speed and kinetic energy of the projectile to decrease more, but in all cases, the

projectile passed through the sample without stopping. The rate of reduction in the projectile speed and kinetic energy in collision with this sample in different percentages of ceramics is seen in Figure (64).

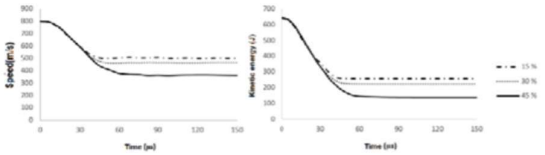

Figure (64) - The graph of the projectile speed and kinetic energy in the sample with 7075 aluminum matrix with a thickness of 20 mm

In the sample with 5083 aluminum matrix and 20 mm thickness, as in the sample with 7075 aluminum matrix, the speed and kinetic energy of the projectile decreased more with increasing the percentage of ceramic, but in all cases, the projectile passes through the sample without stopping. The rate of reduction in the projectile speed and kinetic energy in collision with this sample in different percentages of ceramics is seen in Figure (65).

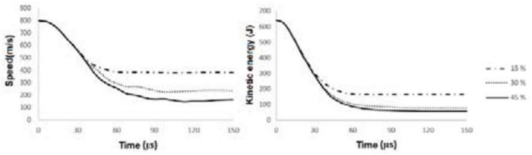

Figure (65) - The graph of the projectile speed and kinetic energy in the sample with 5083 aluminum matrix with a thickness of 20 mm

Effect of ceramic percentage on the speed and kinetic energy of the projectile in collision with samples with a thickness of 25 mm

The reduction rate of speed and kinetic energy of the sample with 6061 aluminum matrix and 25 mm thickness does not change significantly with increasing the percentage of ceramic, and the projectile passes through the sample in all three cases. The rate of reduction in the projectile speed and kinetic energy in collision with this sample in different percentages of ceramics is seen in Figure (66).

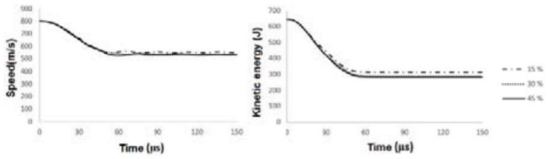

Figure (66) - The graph of the projectile speed and kinetic energy in the sample with 6061 aluminum matrix and 25 mm thickness

The speed and kinetic energy of the projectile decreased more in the sample with 7075 aluminum matrix and 25 mm thickness as the percentage of ceramic increased, such that the sample with 45% ceramic stopped the projectile. But in samples with 15% and 30% ceramic, the projectile passes through the sample without stopping. The rate of reduction in the projectile speed and kinetic energy in collision with this sample in different percentages of ceramics is seen in Figure (67).

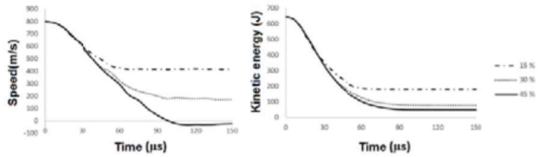

Figure (67) – The graph of the projectile speed and kinetic energy in the sample with 7075 aluminum matrix with a thickness of 25 mm

The effect of ceramic percentage on the speed and kinetic energy of the projectile in collision with samples with a thickness of 30 mm

With increasing the percentage of ceramic in the sample with 7075 aluminum matrix and 30 mm thickness, the speed and kinetic energy of the projectile decreased more, such that the samples with 30% and 40% ceramic stopped the projectile. But in the sample with 15% ceramic, the projectile passes through the sample without stopping. The rate of reduction in the projectile speed and kinetic energy in collision with the sample in different percentages of ceramics is seen in Figure (68).

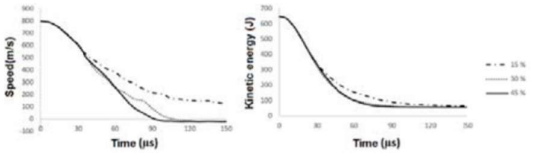

Figure (68) - The graph of the projectile speed and kinetic energy in the sample with 7075 aluminum matrix and 30 mm thickness

In the sample with 5083 aluminum matrix with a thickness of 30 mm in all percentages of ceramic, the projectile stops after impact and penetration in the projectile. with increasing the percentage of ceramic, only the time until the projectile stops in the sample decreases. The rate of reduction in the projectile speed and kinetic energy in dealing with this sample in different percentages is seen in Figure (69).

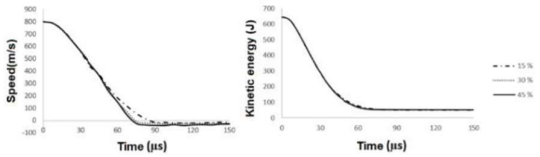

Figure (69) - The graph of the projectile speed and kinetic energy in the sample with 5083 aluminum matrix and 30 mm thickness

The effect of ceramic percentage and alloy type on the projectile penetration depth in samples with a thickness of 20 mm

In samples with a thickness of 20 mm, the projectile completely penetrated and passed through all of them. Therefore, in the samples, increasing the percentage of ceramic and changing the alloy material has no effect on the size of the penetration depth.

The effect of ceramic percentage and alloy type on the projectile penetration depth in samples with a thickness of 25 mm

As shown in Figure (70), in samples with 7075 and 5083 aluminum matrices, the projectile penetration depth decreases with increasing the ceramic percentage. Another noteworthy point in Figure (70) is that the rate of penetration reduction in the sample with 5083 aluminum matrix is higher than the sample with 7075 aluminum matrix. According to Figure (70), it can be seen that the projectile had less penetration in the samples with 7605 aluminum as their base than the other samples.

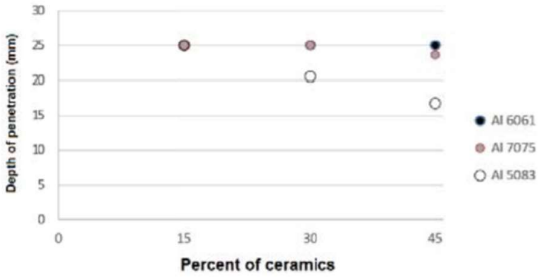

Figure (70) - Projectile penetration depth in samples with 25 mm thickness

The effect of ceramic percentage and alloy type on the projectile penetration depth in samples with a thickness of 30 mm

As shown in Figure (71), in samples with 7075 and 5083 aluminum matrices, the projectile penetration depth decreases with increasing ceramic percentage. According to Figure (71), it is seen that the projectile had less penetration in the samples with 5083 aluminum matrix than the other samples.

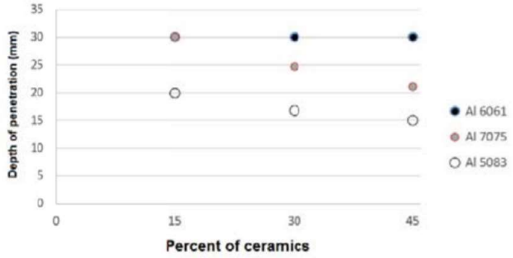

Figure (71) - The projectile penetration depth in samples with a thickness of 30 mm

Effect of ceramic percentage on the projectile residual velocity after penetration in samples with a thickness of 20 mm

As shown in Figure (72), increasing the ceramic percentage in 6061 aluminum matrix samples has little effect on reducing the projectile residual velocity, but in samples with 7075 and 5083 aluminum matrices, it reduces the projectile residual velocity.

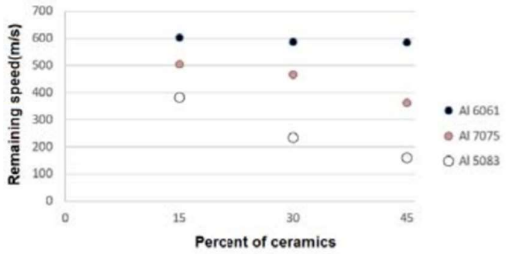

Figure (72) - The projectile residual velocity in samples with a thickness of 20 mm

Effect of ceramic percentage on the projectile residual velocity after penetration in samples with a thickness of 25 mm

As can be seen in Figure (73), increasing the percentage of ceramics in samples with 6061 aluminum matrix does not have much effect on reducing the projectile residual velocity, but in samples with 7075 and 5083 aluminum matrices, it reduces the projectile residual velocity, such that in the sample with 7075 aluminum matrix and 45% and the sample with 5083 aluminum matrix and 30 or 40% ceramic, the projectile stops.

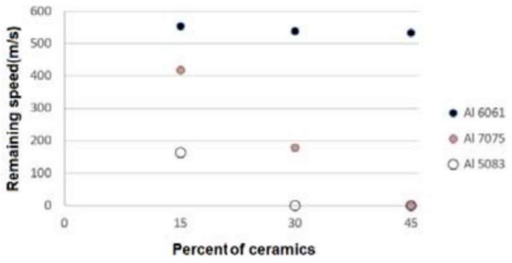

Figure (73) - The projectile residual velocity in samples with 25 mm thickness

The projectile residual velocity after penetration in samples with a thickness of 30 mm

As can be seen in Figure (74), increasing the ceramic percentage in samples with 6061 aluminum matrix has little effect on reducing the projectile residual velocity. However, in samples with 7075 aluminum matrix, it reduces the projectile residual velocity, such that if in the sample with 7545 aluminum matrix that 30 or 45% ceramic is used, the projectile will stop. Samples with 5083 aluminum matrix stop the projectile in all percentages of ceramic.

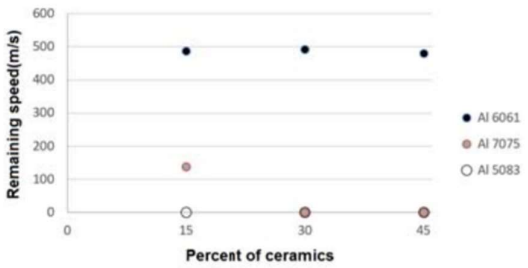

Figure (74) The projectile residual velocity in samples with a thickness of 30 mm

The effect of ceramic percentage on the projectile wear rate after penetration in samples with a thickness of 20 mm

As shown in Figure (75), with increasing ceramic percentage, the projectile wear amount increases. The highest rate of projectile wear after penetration occurred in the sample with 7075 aluminum matrix and 45% ceramic and the lowest rate of projectile wear after penetration occurred in the sample 6061 aluminum matrix and 15% ceramic.

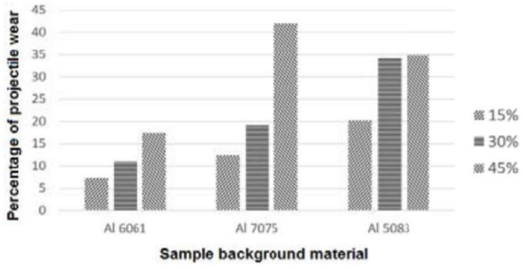

Figure (75) - Projectile wear after penetration in samples with a thickness of 20 mm

Effect of ceramic percentage on projectile wear rate after penetration in samples with a thickness of 25 mm

As shown in Figure (76), the projectile wear amount increases with increasing the ceramic percentage. The highest rate of projectile wear after penetration is in samples with 7075 aluminum matrix and 45% ceramic and samples with 5083 matrix and 45% ceramic. The lowest amount of projectile wear occurred after penetration in the sample with 6061 aluminum matrix and 15% ceramic.

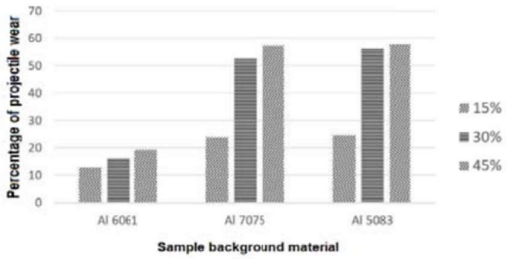

Figure (76) - Projectile wear after penetration in the sample with 25 mm thickness

Effect of ceramic percentage on projectile wear rate after penetration in samples with a thickness of 30 mm

As can be seen in Figure (77), the projectile wear amount increases with increasing ceramic percentage. The highest rate of projectile wear after penetration occurred in samples with 7075 aluminum matrix and 45% ceramic and the lowest rate of projectile wear after penetration occurred in samples with 6061 aluminum matrix and 15% ceramic.

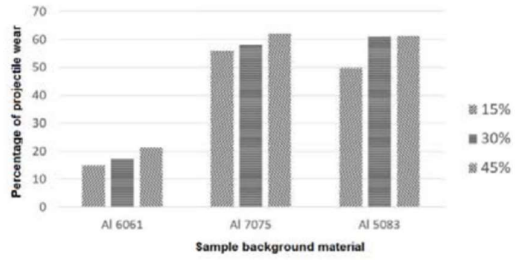

Figure (77) - Projectile wear after penetration in samples with a thickness of 30 mm

Optimal sample

As per the ground force ballistic limit criteria, a sample's ballistic performance is acceptable provided the penetration damage caused by the projectile on its back surface does not allow light to pass through. The GOST standard is one of the standards in the back surface mark criteria (deformation of the back surface). Regardless of the deformation of the sample surface, the ballistic performance of this sample is approved in this standard as long as it deforms less than 16 mm upon hitting the sample with the 39 * 7.62 projectile and penetrating it. The sample with a thickness of 25 mm and 30% ceramic and 5083 aluminum matrix meets the standard criteria. It is because the deformation of the sample back surface is 3.41 mm and the penetration in it is such that the sample is not perforated and light does not pass through it. As opposed to other samples in which the projectile was stopped, this one had the lowest weight and thickness.

Experimental test results

Viewing the images of the damaged areas, the experimental samples of the ballistic test of them are compared to the standard steel sample.

Experimental samples after ballistic evaluation

Figures (78), (79), and (80) show the front and back surfaces of the experimental samples after ballistic evaluation.

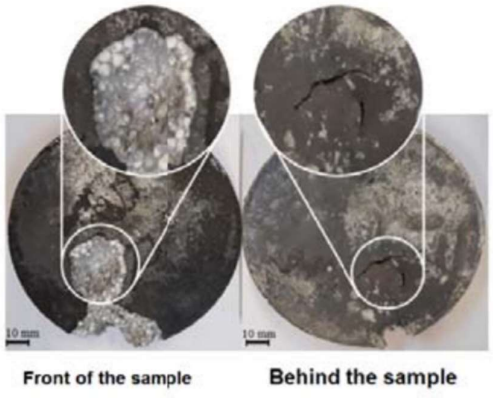

Figure (78) - The first experimental sample

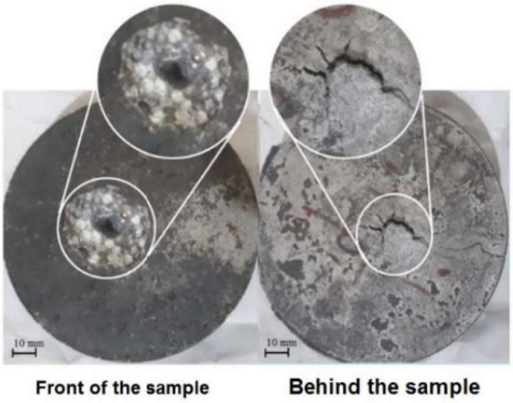

Figure (79) - The second experimental sample

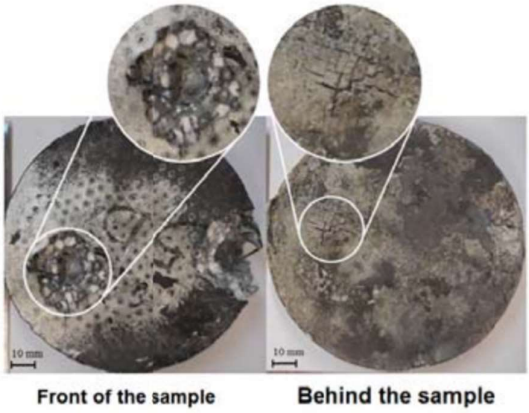

Figure (80) - The third experimental sample

Table (2) shows the effective parameters in experimental samples' ballistic performance and how they compare with the standard integrated steel sample. According to Table (2), the mass effect of experimental samples is between 1.63 and 1.68. In other words, the samples are about 40% lighter than the monolithic steel armor.

Table (2) - Ballistic performance parameters of experimental samples

	Weight (kg)	Surface density (kg/m^2)	Mass effect
monolithic steel armor	------	114	1
first sample	0.651	68.50	1.66
second sample	0.663	69.76	1.63
third sample	0.642	67.55	1.68

Ballistic performance of experimental samples

The ballistic performance of experimental samples is examined in this section from the two perspectives of the ground force ballistic limit and the back surface mark (deformation of the back surface).
As a result of the ballistic evaluation of the experimental samples, it was determined that their ballistic performance was acceptable based on the ground force ballistic limit criterion because no light passed through the protrusions and cracks on the back of the samples. Furthermore, the deformation of the back surface of all samples was between 2 to 4 mm, so based on the criterion of deformation of the back surface, the ballistic performance of the samples is also confirmed.

Comparison of simulation and experimental test results

In Table 3, you can see the projectile penetration depth in each of the samples, along with the percentage difference between experimental and numerical results. In view of the results obtained, they are in good accordance with one another.

Table (3) - Comparison of simulation and experimental test results

	Projectile penetration depth (mm)	Percentage difference between experimental and numerical results (%)
The simulated sample (numerical)	20.57	-------
first sample	18.65	9.33
second sample	19.20	6.67
third sample	18.35	10.79

According to the following, there are a number of reasons why the numerical method and the experimental field produce different results.
- Projectile speed in the simulation is a little higher than the experimental projectile speed.

- Due to the geometric complexity of the experimental sample and meshing limitations, ceramic reinforcements in the simulation are further apart than in the experimental sample.

- As the experimental evaluation was conducted with a real weapon, there is a possibility of human error, such as the projectile not hitting the surface at a 90-degree angle.

Furthermore, the properties of materials are not entirely consistent between simulation and reality.

Conclusion

As observed in this study, percentage effects of ceramics and matrix alloy material and thickness on the ballistic performance of composite samples were investigated. 6061, 7075, and 5083 aluminum were used in this research, with ceramic percentages of 30, 15, and 45. 20, 25, and 30 mm are the thicknesses of the examined samples. The results showed that among the various alloys used, samples with 5083 aluminum matrix had the best ballistic performance, and samples with 6061 aluminum matrix had the worst ballistic performance. Increasing the ceramic percentage and thickness in samples with 7075 and 5083 aluminum matrices

causes a significant reduction in the residual velocity. However, in samples with 6061 aluminum matrix, due to its lower impact resistance than other alloys, it does not have much effect in reducing the residual velocity. Additionally, the penetration depth decreased with increasing the percentage of ceramics in samples where the projectile was stopped. In these samples, the penetration depth of samples with 5083 aluminum matrix is less than that of samples with 7075 aluminum matrix. Another finding of the observations is that the residual velocity decreases with increasing projectile wear. In conclusion, the following results were obtained:

5083 aluminum has the best ballistic performance.
With increasing the ceramic percentage in samples with 7075 and 5083 aluminum matrices, the residual velocity decreases significantly.

The penetration depth has decreased with increasing ceramic percentage in samples in which the projectile stopped.

Samples with 5083 aluminum matrix penetrate deeper than samples with 7075 aluminum matrix after the projectile has been stopped.
In samples with 6061 aluminum matrix, the residual velocity does not decrease significantly with increasing thickness.

In the process of penetration, the residual velocity of the projectile decreases as the projectile wears out.
The penetration depth decreases as the thickness increases in samples where the projectile has stopped, while other conditions remain constant.
Due to the monolithic nature of the ceramic layer, there was a limitation in prior research that it could only be shot once. By using microspheres of ceramic as reinforcements, this research gap has been eliminated in this research. Additionally, most of the samples presented in the past are layered, but according to researchers, if the sample is monolithic, it will have better ballistic performance. By designing and manufacturing monolithic composite armor, this problem was solved in this research.

References

[1] Lashgari, H., Emami, M., "Investigation of the effect of strontium on the microstructure of cast A613- B4C composites," In Persian, Foundry Quarterly, pp. 9–11, 1697.
[2] Silva, M. V., Stainer, D., Al-Qureshi, H. A., Montedo, O. R. K. and Hotza, D., "Alumina-Based Ceramics for Armor Application: Mechanical Characterization and Ballistic Testing," J. Ceram., Vol. 9014, pp. 1–3, 2014.
[3] Rashed, A., Yazdani, M., Babaluo, A. A., Hajizadeh Parvin, P., "Investigation on high-velocity impact performance of multi-layered alumina ceramic armors with polymeric interlayers," J. Compos. Mater. Vol. 10, No. 91, pp. 6131–6173, 2011.
[4] Iqbal, M. A., Senthil, K., Sharma, P., Gupta, N. K. "An investigation of the constitutive behavior of Armox 100T steel and armor piercing incendiary projectile material," Int. J. Impact Eng., vol. 96, pp. 146–164,2016.
[5] Venkatesan, J., Iqbal, M. A., Madhu, V., "Ballistic Performance of Bilayer Alumina/Aluminium and Silicon Carbide/Aluminium Armours," Procedia Eng., Vol. 176, pp. 371–379, 2017.
[6] Cui, F., Wu, G, Ma, T., Li, W., "Effect of ceramic properties and depth-of penetration test parameters on the ballistic performance of armour ceramics" Def. Sci. J., Vol. 37, No. 6, pp. 930–939, 2017.
[7] Liu, J., Wu, C., Li, J., Fang, J., Su, Y., Shao, R., "Ceramic balls protected ultra-high-performance concrete structure against projectile impact–A numerical study," Int. J. Impact Eng., Vol. 191, pp. 146–139, 2018.
[8] Seifert, W., Strassburger, E., Dolak, M., Schaare, S., "Experimental study on the dependency of the ballistic performance of tiled ceramic/metal targets on inter tile gap width and projectile impact position," Int. J. Impact Eng., Vol. 199, pp. 10–18, 2019.
[9] An, X., Tian, C., Sun, Q., Dong, Y., "Effects of material of metallic frame on the penetration resistances of ceramic-metal hybrid structures," Def. Technol., pp. 1–11, 2018.
[10] Tian, C., Sun, Q., An, X., Ye, P,. Dong, Y., "Influences of ceramic constraint on protection performances of ceramic-metal hybrid structures under impact loads," Int. J. Mech. Sci., Vol. 118, No. February, pp. 91–80, 2018.
[11] Fras, T., Roth, C. C., Mohr, D., "Dynamic perforation of ultra-hard high-strength armor steel: Impact experiments and modeling," Int. J. Impact Eng., vol. 131, pp. 256–271, 2019.
[12] Forrestal, M. J., Børvik, T., Warren, T. L., "Perforation of 7071-T311 Aluminum Armor Plates with 7639 mm APM9 Bullets," Exp. Mech., pp. 1941–1911, 2010.
[13] Wen, H. M., He, Y., Lan, B., "A combined numerical and theoretical study on the penetration of a jacketed rod into semi-infi nite targets," Int. J. Impact Eng., pp. 884–1010, 2011.
[14] Crouch, I. G., "the Science of Armour Materials," Duxford, 2013.